Charge-state equilibration length of a highly charged ion inside a carbon solid

R. Herrmann,[1] C. L. Cocke,[2] J. Ullrich,[3] S. Hagmann,[2] M. Stoeckli,[2] and H. Schmidt-Boecking[1]
[1]*Institut für Kernphysik, Universität Frankfurt, August Euler Straße 6, 60486 Frankfurt am Main, Germany*
[2]*J. R. Macdonald Laboratory, Kansas State University, Manhattan, Kansas 66506*
[3]*Gesellschaft für Schwerionenforschung mbH, Planckstraße 1, 64220 Darmstadt 11, Germany*
(Received 1 December 1993)

The penetration of 576-keV Ar^{q+} ions with initial charge states $q_i = 8,12,16$ through a carbon foil of 310 Å thickness has been investigated. The projectile's energy loss and final charge-state distribution have been measured. Within a resolution of a few percent no dependence of these data on the projectile's initial charge state was found. Furthermore the relative yield of Auger electrons emitted by the projectile before and after the foil was detected. From these yields we could derive that the Ar ions quickly reach an equilibrium excitation state inside the foil that does not depend on the initial charge state q_i. From the measured energy-loss data we derive an upper limit for the projectile's average charge-state equilibration length x_e inside the foil of approximately one carbon layer. This result implies extremely large cross sections for electron transfer mechanisms between projectile and solid. An estimation of this cross section by using the classical over-barrier model hardly explains the observed, very large charge-exchange cross sections between ion and solid.

PACS number(s): 79.20.Nc, 34.50.Bw, 61.80.Mk

INTRODUCTION

The interaction of slow, highly charged ions with conducting solids and surfaces has attracted great interest in the past few years. Most experiments that have been done in that field deal with the investigation of Auger electrons[1–11] and characteristic x rays[12–17] that are emitted by the projectile when it interacts with a conducting solid. Also the yield and the statistics of low-energy secondary electrons emitted during the interaction of ions in various charge states with metal surfaces have been studied in detail.[18–27] Especially the results of the latter investigations seem to depend very sensitively on the surface conditions and therefore most experiments have been performed in an ultrahigh vacuum environment. The typical range of projectile velocity (v_p) that has been investigated in these experiments is $0.001 \text{ a.u.} \leq v_p \leq 1 \text{ a.u.}$

According to the present understanding of the interaction between a highly charged ion and a conducting surface, resonant transfer of electrons from the surface conducting band into highly excited Rydberg states of the ion (typically $n \geq 7$) is the dominant process that opens the interaction "scenario"at typical ion-surface distances of several tens of angstroms (depending on the ion's initial charge state and the work function of the solid).[25,26] Within a very short time [typically few times 10^{-16} sec (Ref. 14)] this so-called "resonant neutralization" process forms a neutral atom with many electrons in highly excited states for which the name "hollow atom" has been established. These Rydberg electrons can cascade to lower levels radiatively or via emitting Auger electrons. Various groups have shown that due to the lack of time between the projectile's first electron capture and its penetration into the solid, only few electrons can reach the projectile's inner shells in a decay cascade in front of the surface.[3–5,10,11] It was found that, even for very slow projectiles ($v_p < 5 \times 10^{-3}$ a.u.), the yield of fast projectile Auger electrons, which are emitted in front of the surface, does not exceed a fraction of about 10% of the total fast projectile Auger electron yield.[10] This saturation effect indicates the projectile's acceleration by its image charge in front of the surface.

The subject of the present article is the investigation of charge transfer between a moderate velocity ($v_p = 0.76$ a.u.) highly charged ion and a solid when the ion traverses through the solid. Essentially all inner-shell vacancies should, according to the results described above, survive up to the ions penetration into the solid.

As soon as the hollow projectile enters the solid all highly excited Rydberg electrons are "peeled off"[27,25] due to the screening of the projectile core by electrons from the solid. The electrons in the outermost remaining states can still populate inner shell orbitals by cascading Auger and radiative decay processes. Besides these processes, a variety of charge-exchange mechanisms may become active. For example, interaction of the projectile's loosely bound outer electrons with the nuclei and electrons of the solid can transfer the projectile electrons into the continuum or into lower-n projectile states. The latter process, which could be considered as a "Coulomb force nonradiative deexcitation" can be expected to be less likely than the aforementioned because, in contrast to the electron loss, it requires a well-defined energy transfer to the projectile electron and also the number of final electronic states is much smaller. Furthermore, inner-shell quasimolecular electron transfer between the projectile and the target can occur. According to results from ion-atom collisions,[28] the cross section for this charge-exchange mechanism in the solid can be expected to vary strongly with the binding energy of the related electronic states and the projectile velocity.

After a certain penetration depth x_e the combined

efforts of these competing processes should create a dynamic charge and excitation state equilibrium of the projectile. Depending upon the strength of the described mechanisms, the projectile's dynamic charge-state distribution inside the solid might strongly depend on the number of its inner-shell vacancies.

The central point of interest in the present investigation is to obtain information on the equilibration length x_e of a moderate velocity highly charged ion penetrating into a solid. This information can be very important for the application of highly charged ions to surface modification, since it allows one to estimate how deep below the surface a highly charged ion can transport some fraction of its potential energy into the solid. A very sensitive method to determine the equilibration length x_e of an ion inside a thin solid is the measurement of its energy loss in the solid as a function of its initial charge state q_i. The differential electronic energy loss $(dE/dx)_e$ of a charged projectile at a particular position x in a conducting solid is proportional to the square of its effective charge state $q_{\text{eff}}(x)$.[29] Therefore the projectile's electronic energy loss ΔE in a thin solid target is an integral measure of its charge-state evolution in the solid. If the projectile's effective charge state $q_{\text{eff}}(x)$ is different for a few target layers for different incoming charge states q_i, the projectile's electronic energy loss ΔE in a thin foil should show variations with q_i. As will be shown later, nuclear stopping arises predominantly from very close collisions between the projectile and the solid atoms, and thus only the population of the innermost electronic orbitals may influence weakly the projectile's nuclear energy loss.

In the present experiment the energy loss of 576-keV Ar^{q+} ions ($v_p = 0.76$ a.u.) passing a 310-Å carbon foil has been measured for incoming charge states $q_i = 8, 12, 16$. According to calculations with the TRIM computer code,[30] in this collision system electronic stopping contributes about 75% to the projectile's total energy loss while nuclear stopping contributes about 25%. Therefore a possible q_i dependence of the contributing electronic stopping should clearly be displayed by the total energy loss. As will be shown later, the measurement is sensitive enough to determine the projectile's equilibration length x_e with an accuracy of a few angstroms. In addition, the distribution of final ion charge states has been determined for the two initial projectile charge states $q_i = 8, 16$.

Finally, the relative yield of projectile Auger electrons and photons emitted by the projectile near the entrance and exit surface of the foil was measured as a function of $q_i = 8, 12, 16$. A comparison of the entrance and exit yields as a function of q_i allows the determination of whether the projectile reaches an inner-shell equilibrium excitation state in the foil.

EXPERIMENTAL SETUP AND DATA REDUCTION

The experiment was performed at the CRYEBIS ion source of Kansas State University. Figure 1(a) shows a sketch of the experimental setup. A beam of Ar^{q+} ions was extracted from the CRYEBIS ion source and transported through a beamline of an approximate length of 5 m to the scattering chamber in which the carbon foil was mounted. By using several turbomolecular vacuum pumps and conductance limiters between the beamline and the scattering chamber, the beamline could be kept in the low-10^{-8}-mbar vacuum range while the scattering chamber was at 1×10^{-6} mbar. Since the beam had to pass only about 20 cm through the 10^{-6}-mbar vacuum before hitting the foil, charge exchange between the Ar projectiles and the residual gas atoms was small. Two sets of slits in front of the scattering chamber collimated

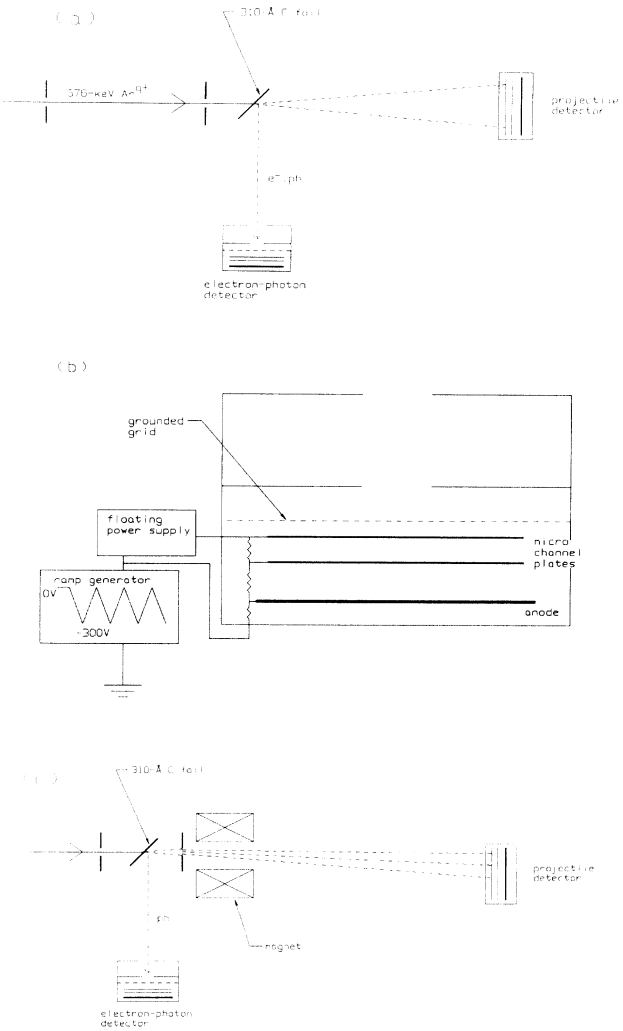

FIG. 1. (a) Sketch of the experimental setup. The real distance between the foil and the projectile detector was 22.3 cm, while the foil-electron detector distance was about 6.5 cm. (b) Schematic drawing of the electron detector. In order to keep the potential difference between the two channel plates and between the lower channel plate and the anode constant while varying the repelling voltage between the upper channel plate and the grid, the high voltage for the channel plate and the anode was provided by a floating power supply, which was driven by a ramp generator. (c) Sketch of the experimental setup for resolving the final projectile charge states. The distance between the foil and the projectile detector was 3 m.

the beam to a spot 1×1 mm^2 in size and an angular divergence of less than 1 mrad.

After passing the carbon foil the scattered projectiles were detected at a distance of 22.3 cm by a two-dimensional position-sensitive channel-plate detector. This allowed the measurement of the angular distribution of the outgoing projectiles. The position information was obtained by using a "wedge and strip" anode.[31]

A second (nonposition-sensitive) channel-plate detector was mounted at a distance of 7 cm below the carbon foil, perpendicular to the beam axis, for detecting electrons and photons emitted by the foil or the projectile behind or in front of the foil. In order to be able to observe decay processes at the entrance and exit surface of the foil separately, the carbon foil could be oriented relative to the beam and the electron detector so that only electrons from one of the carbon surfaces (either entrance or exit) could reach the detector at a time. Henceforth the foil orientation that allowed the observation of the entrance surface will be denoted "position 1," in contrast to "position 2," which denotes the foil position in which exit surface electrons were detected.

A grounded high-transmission grid was mounted at a distance of about 1 cm in front of the electron detector's upper channel plate. By applying a negative voltage up to -300 V to the front side of the upper channel plate, an energy limit for the detected electrons could be set. Thus the electron detector worked approximately as a retarding grid spectrometer. In order to keep the channel-plate gain independent of the electron energy while varying the repelling voltage, the high voltage for both channel plates and the anode of the electron detector was provided by a floating power supply that was driven by a grounded ramp generator [see Fig. 1(b)]. The scattered projectiles and the electrons (photons) were measured in coincidence by using standard NIM electronics. Here the electron (photon) detector signal was used as the start while the projectile signal stopped the time measurement. Figure 2 shows a typical coincidence spectrum obtained with start signals when the foil is in position 2. The spectrum contains two peaks, a broad one centered near 130 ns that covers a large range of time differences between the start and the stop and a narrow one near 140 ns. It was found that the intensity of the narrow peak did not depend on the repelling voltage of the electron detector whereas the broad peak did. Furthermore the time difference between the narrow peak and the right falling edge (higher channels) of the broad peak is about 3–4 nsec. This is typically the time in which a 300-eV electron passes the distance between the foil and the start detector. Therefore we assume that the narrow peak at larger time coordinates is created by coincidences between photons and outgoing Ar ions, while the broad peak is due to electron-ion coincidences. The flight time spectrum obtained with the foil in position 1 does not show the photon peak.

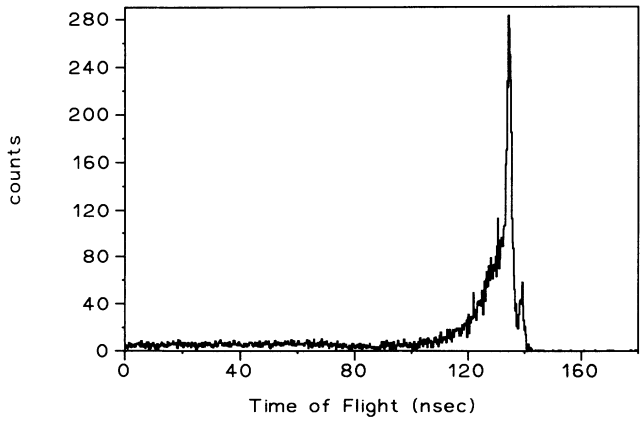

FIG. 2. Time-of-flight spectrum between electrons (photons) and outgoing projectiles with the foil in position 2 for an incoming Ar^{16+} ion. The broad peak on the left-hand side represents the electron-projectile coincidences while the small narrow peak on the right-hand side is due to photon-projectile coincidences.

Time spectra were created for five different projectile scattering angle regimes. Using the actual distances between the carbon foil and the projectile detector for each scattering angle, the time spectra were transformed into ejectile kinetic-energy spectra. The projectile's kinetic energy after leaving the foil was obtained from the position of the photon peak centroid in the coincidence spectrum. The width of the photon peak reflects the ejectiles energy straggling, while the electron peak width results from a superposition of the energy distributions of outgoing projectiles and electrons. A comparison between the peaks shows that the width of the electron peak is dominated by the electron's energy distribution.

The projectile's energy loss when passing the foil was determined by the incoming beam energy minus the projectile's kinetic energy after leaving the foil. The flight time of a 576-keV Ar ion between the foil and the projectile detector is about 140 nsec. As will be seen later, the typical energy loss of the Ar projectiles in the carbon foil is 40 keV. For the distance between the foil and the projectile detector this energy loss corresponds to a flight time difference relative to the initial beam of about 5 nsec. Even though the electronic time resolution allowed determination of the time difference between a photon and a scattered projectile with an accuracy of only about 1.5 nsec—corresponding to an energy accuracy of about 10 keV—the centroid of the projectiles' flight time distribution could be determined about 10 times more accurately. In order to measure precisely the corresponding flight time of the incoming Ar beam for the distance between the projectile detector and the foil, the latter could be replaced by a well collimated air gas jet. In single collisions with the air atoms, the highly charged ions have a large chance to capture electrons in excited states which can lead to photon or electron emission via radiative or Auger decay of the excited Ar states. These gas collisions are not accompanied by a significant energy loss of the projectile. Thus a coincidence between such a photon and the scattered projectile allows us to deduce the Ar beam time of flight between the gas jet center and the projectile detector with an accuracy of about 0.2 nsec. In order to transform the gas-foil flight time difference into an absolute energy loss with an accuracy of 1 keV, the spatial distance between source points

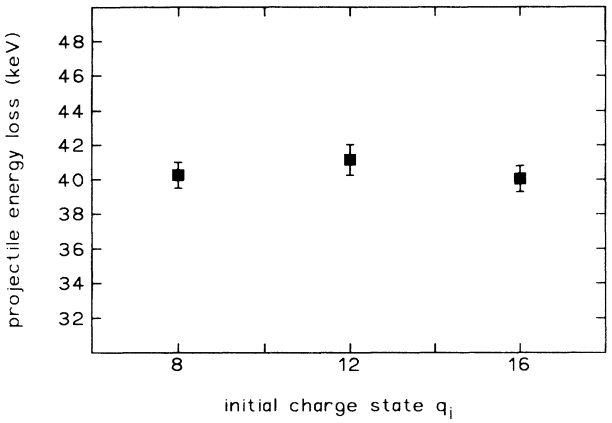

FIG. 3. Spectrum of the Ar ions' energy loss after passing the carbon foil integrated over all scattering angles as a function of the initial charge state q_i.

for the jet and the foil exciters has to be known with a precision of 0.2 mm.

The accuracy achieved in the experiment for the difference of these positions was 3 mm, corresponding to an uncertainty in the absolute energy loss of 14 keV. However, the error in the relative projectile's energy loss for different projectile charge states does not include the above-described uncertainties of the involved spatial distances since those uncertainties are systematic errors that are constant for all projectile charge states. Without taking these systematic errors into account, the projectile's relative energy loss in the carbon foil as a function of q_i was obtained with an accuracy of about 2 keV. In order to determine the projectile's equilibration length in the carbon foil, it is the relative energy loss as a function of the projectile's initial charge state rather than the absolute value of energy loss that matters. Therefore the error bars shown in Figs. 3 and 4 do not include the described systematic error and should be considered "relative" errors in the sense described above.

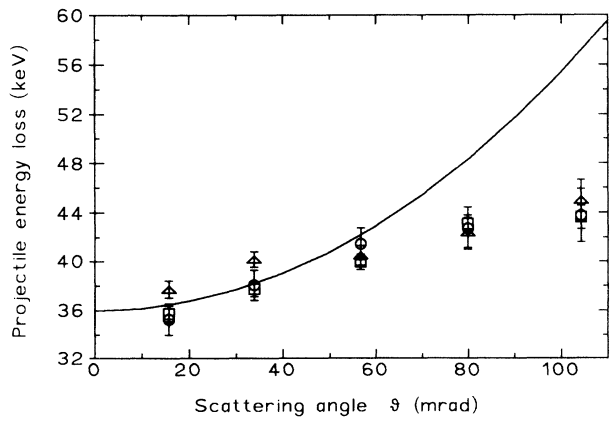

FIG. 4. Spectrum of the projectiles' energy loss as a function of the scattering angle. The different symbols represent the following incoming ions: squares: Ar^{8+}; triangles: Ar^{12+}; circles: Ar^{16+}. The error bars at the data points represent relative errors as described in the text. The solid line shows the calculated dependence of the projectile kinetic energy loss on the scattering angle in single collisions between Ar projectiles and C atoms.

For measuring the Ar ions' final charge-state distribution after leaving the foil, the apparatus was modified as shown in Fig. 1(c). At a distance of about 10 cm behind the C foil a third set of slits collimated the ejectiles' horizontal scattering distribution to a narrow slice of 1 mm width. Directly behind those slits a vertical magnetic field horizontally separated the outgoing projectile charge states. The final projectile charge-state distribution could be resolved by a position sensitive detector mounted 3 m behind the magnet.

RESULTS AND DISCUSSION

Figure 3 shows the total energy loss ΔE of the Ar projectiles in a 310-Å carbon foil, integrated over all scattering angles, as a function of their initial charge state q_i. Within the error bars no q_i dependence of the energy loss can be observed. In Fig. 4 the energy loss as a function of the scattering angle $\Delta E(\theta)$ is presented for each initial q_i. No significant energy loss difference between the incoming charge states can be observed. A clear increase of the energy loss with increasing projectile emergence angles was found for every investigated initial charge state. Ar ions that leave the foil in a narrow cone around 0° did not exchange a significant amount of transverse momentum with any C atom by nuclear stopping. Thus those ions are assumed to have mainly lost their energy in collisions with electrons. Projectile emergence angles significantly larger than 0° can be reached in either close single or multiple collision events with the solid atoms. The full line in Fig. 4 is calculated as the sum of energy loss for emergence angles around 0° plus the kinematic energy transfer of Ar projectiles to a single C atom for a two-body elastic scattering by an angle θ. As can be seen, the calculated curve shows clearly a steeper slope than the measured data. For large scattering angles the calculated "two-body" energy loss is up to two times larger than the measured one.

It can be calculated that, for scattering to the same final scattering angle, the total kinetic energy that is transferred from the projectile to the target in many successive small-angle collisions is smaller than that obtained in one large-angle single collision. This suggests that the measured scattering distribution up to 110 mrad is dominated by multiple-scattering processes between projectile and target atoms rather than single-scattering events. This conclusion is in agreement with that expected from the calculations by Sigmund and Winterborn,[32] who showed that the scattering distribution of ions passing thin solids is dominated by multiple-scattering events of the projectile with the solid atoms up to scattering angles of several times the full width at half maximum of the scattering distribution. Only projectile scattering angles larger than about 10 times the half-width of the scattering distribution are more likely reached by single-scattering events.

For a quantitative comparison of the half-width of the measured scattering distribution with an estimate obtained by the Sigmund-Winterborn formalism, the foil

thickness is a sensitive parameter. Therefore the accuracy of the manufacturer's declaration concerning the carbon foil thickness was checked by using the TRIM computer code[30] to numerically simulate the scattering distribution of Ar ions in a carbon foil as function of the foil thickness. The carbon foil was labeled to be a 3-μg/cm^2 foil. If one assumes a foil density of 1.65–2.5 g/cm^3 one can calculate a foil thickness of about 120–215 Å. Taking into account that the foil was tilted by an angle of 20°, the effective foil thickness that was passed by the Ar ions is 128–229 Å. The simulated distributions were folded with the experimental resolution, which was determined by the beam diameter and the position resolution of the projectile detector. Figure 5 shows the measured scattering distribution for initial Ar^{16+} ions in comparison with TRIM simulations for two different target thicknesses. As can be seen, the measured distribution matches very well the calculated one for an assumed target thickness of 310 Å, whereas the calculated distribution for a thickness of 120 Å is by far too narrow. Furthermore the measured average energy loss of 40 keV could also be reproduced by TRIM calculations when assuming a foil thickness of 310 Å. The TRIM code does not take into account the projectiles initial charge state. Since it was found that in the investigated velocity regime the projectile's initial charge state does not affect its energy loss, we expect the calculations to be a realistic description of the measurement. Therefore the foil thickness was taken to be 310 Å.

From the Sigmund-Winterborn formalism, one can estimate the half-width for the scattering distribution of 576-keV Ar ions passing a 310-Å C foil to be about 24 mrad. As can be seen from Fig. 5, the measured half-width is about 27 mrad, which is fairly close to the estimated Sigmund-Winterborn half-width. Thus the investigated range of projectile scattering angles is clearly within the regime that is dominantly described by multiple-scattering events. This is in agreement with the assumption taken from the shape of the $\Delta E(\theta)$ curve.

The measured independence of the projectile's energy loss of its initial charge state q_i is in agreement with the findings for the projectile's final charge-state distribution as function of q_i. As expected from the energy-loss data no dependence of the distribution of outgoing Ar charge states (q_o) on the initial charge state q_i was found. Figure 6 shows the final charge-state distribution of Ar ions after leaving the foil for the incoming Ar charge states $q_i=8$ and 16. The two distributions are essentially equal for both initial charge states and both cases produce an average final charge state of $\bar{q}_0 \approx 2.2$.

The foil thickness of about 310 Å is roughly equivalent to about 150 C-atom layers. Thus from the integral energy loss we derive that the Ar ion loses on the average 130 eV/Å or 267 eV/layer. The calculation below shows that the information of the average outgoing charge state in combination with the relative accuracy that was achieved for the projectile's energy loss as function of q_i allows a determination of the projectile's charge equilibration length (x_d) with an accuracy of less than one carbon layer.

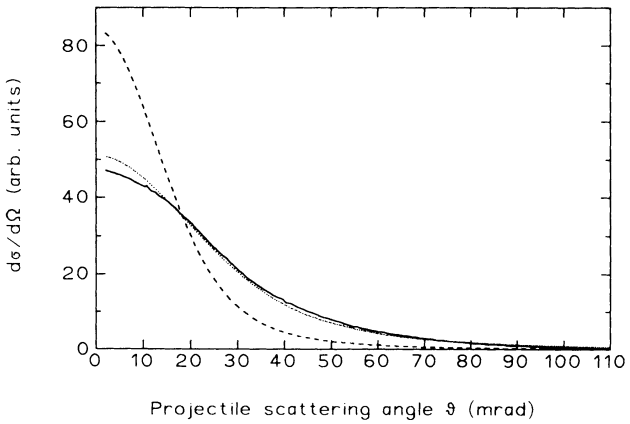

FIG. 5. Measured distribution of projectile scattering angles in comparison with scattering distributions calculated with the TRIM computer code for two different target thicknesses. The solid line represents the measurement, the dotted line shows the result of the TRIM calculation for a foil thickness of 310 Å, and the dashed line represents the TRIM calculation for a foil thickness of 120 Å.

In Fig. 7 a possible shape of the projectile's $q(x)$ function in the solid is shown schematically. (Here x denotes the ions penetration depth inside the carbon foil.) Since the exact shape of this function is not known, we assume an exponential decrease of the projectile's charge state $q(x)$ from q_i into q_o with mean length x_d:

$$q(x)=q_o+(q_i-q_o)e^{-x/x_d} , \tag{1}$$

where q_o is the Ar equilibrium charge state.

In the low projectile velocity regime that is investigated in the present experiment, the projectile cannot be treated as a point charge. Therefore its effective charge state, which determines its energy loss in the solid, depends on the radius of the screening electron cloud around the projectile at each position in the solid. This radius might change rapidly with the ion's increasing penetration depth especially at the entrance of the solid, where the projectile's excitation state is far from being relaxed. According to a semiempirical treatment of Brandt,[29,35] which is discussed below, an effective ion charge state can be defined such that the projectile's energy loss at each position in the solid is a function of the square of its effective charge.

Thus we obtain

$$\begin{aligned}\Delta E(q_i,x_o)&=\int_o^{x_o} c\,q(x)^2dx \\ &=c\int_o^{x_o}[q_o+(q_i-q_o)e^{-x/x_d}]^2dx \\ &=c[(q_i-q_o)^2(x_d/2)(1-e^{-(2x_o/x_d)})+2q_o(q_i-q_o)x_d(1-e^{-(x_o/x_d)})+q_o^2x_o] .\end{aligned} \tag{2}$$

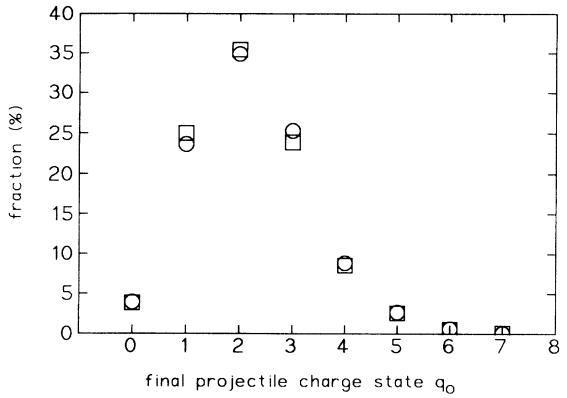

FIG. 6. Distribution of final projectile charge states q_o for the incoming charge states $q_i=8+$ (squares) and $q_i=16+$ (circles).

Here x_o describes the foil thickness and c denotes the proportionality between the ions energy loss and the square of its charge. In our model, which assumes an exponential decrease of the projectile's effective charge state, we treat the equilibrium length x_d as a constant of the particular ion-solid system, such that x_d does not depend on q_i, although a more sophisticated model would certainly take some q_i dependence of x_d into account.

Since we observed no q_i dependence of the projectile's energy loss within the accuracy of our measurement, x_d must be very small relative to x_o. Therefore we approximate

$$(1-e^{-(2x_o/x_d)})\approx(1-e^{-(x_o/x_d)})\approx 1 . \quad (3)$$

This leads to

$$\Delta E(q_i,x_o)=cx_oq_o^2+cx_d\Delta q(\Delta q/2+2q_o)$$
$$\text{with } \Delta q=(q_i-q_o) . \quad (4)$$

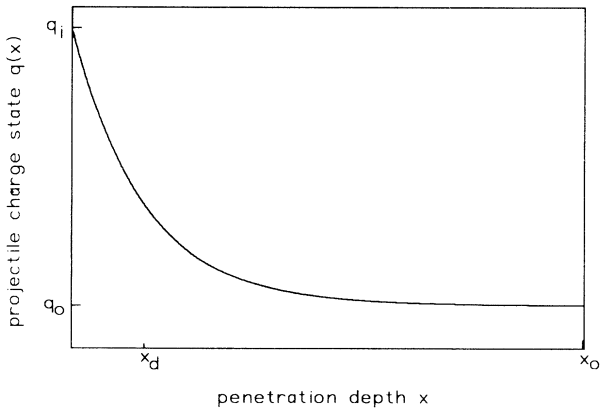

FIG. 7. Schematic drawing of the projectile's effective charge state inside the carbon foil $q(x)$ as a function of the penetration depth x. q_i and q_o describe the projectile's initial and final charge states. x_o denotes the foil thickness and x_d is the position where $q(x)$ is given by $q(x_d)=q_o+e^{-1}(q_i-q_o)$.

The data on the projectile's average energy loss including the error bars (Fig. 3) show that the maximum possible energy-loss increase as a function of q_i is 2 keV between $q_i=8+$ and $16+$. This yields a maximum value for $x_d=0.0022x_o$ or $x_o=0.68$ Å (0.33 atomic layers).

Figure 8(a) shows, for each of the three incoming charge states, the electron yields from the entrance side of the C foil for three different repelling voltages V_R. As mentioned earlier, the time-of-flight spectrum taken with the foil in position 2 (exit side) allowed us to separate between photon and electron yields. Therefore Figs. 8(b) and 8(c) show the electron and photon yields from the exit side of the foil separately. Only relative yields are shown as the absolute efficiency and the solid angle of the electron detector was not known. Each yield is normalized to the same number of projectiles, which allows a quantitative comparison of scales of the three spectra of Fig. 8.

The maximum kinetic energy that can be transferred from a 576-keV Ar ion to an electron at rest in a classical "head-on collision" is $E_{\text{kin}}=31.4$ eV. Thus the observed "high-energy" electrons ($E_e\geq 100$ eV) cannot be kinetically emitted, but can only be produced in some type of potential emission, which means that their kinetic energy is taken from the potential energy which the ion has carried into the system. According to the statements in the Introduction it can be assumed that the observed entrance side electrons originate almost exclusively from subsurface projectile Auger emission processes which follow electron transfer from the solid into excited ionic states. This assumption is supported by the observation that the electron yield from the entrance surface clearly increases with increasing q_i. First, the potential energy that is carried by the incoming ion grows with q_i and second, the number of possible Auger transitions from highly excited atomic levels into inner shells also increases with rising q_i. In Fig. 8(a) the relative increase of the Ar potential energy as a function of q_i, $E_{\text{pot}}(q_i)$, is also shown. The shapes of the curves are very similar. Due to the electron energy range scanned by the repelling voltage, we assume that mostly Ar L Auger electrons are detected. Since those electrons can already be measured for incoming Ar^{8+}, which does not carry L-shell vacancies, we conclude that a small number of Ar L vacancies are created by excitation processes in the foil. Those vacancies lead to a finite fraction of q_i independent electron yield.

In contrast to the entrance side result, the exit side yield does not depend on q_i at all. When trying to understand the behavior of the exit side yield, one first has to ask whether electrons that are emitted close to the foils entrance surface can penetrate through the foil and be detected at the exit side. This can be excluded since the results of electron transmission measurements through thin foils[33] show that electrons with initial energies up to $E_e=600$ eV are stopped in a 310-Å carbon foil. Therefore we assume that the exit side electrons originate from Auger processes in the outgoing projectile. Since the electron exit yield does not depend on q_i, the ion obviously reaches the exit surface of the foil in some equilibrium

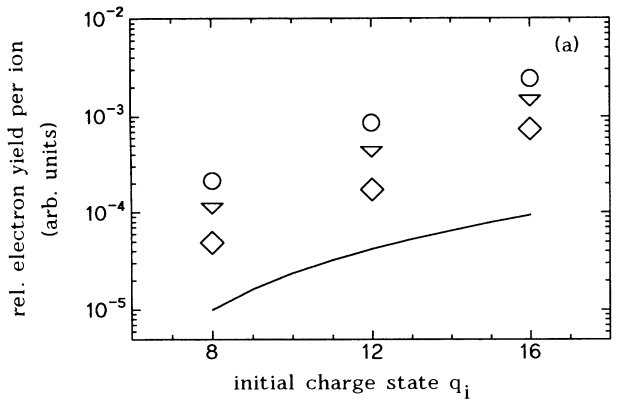

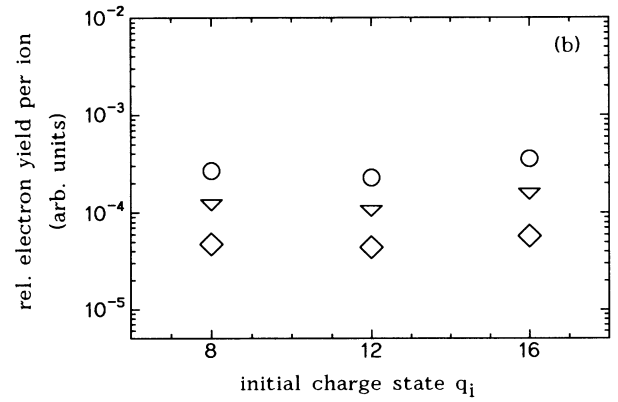

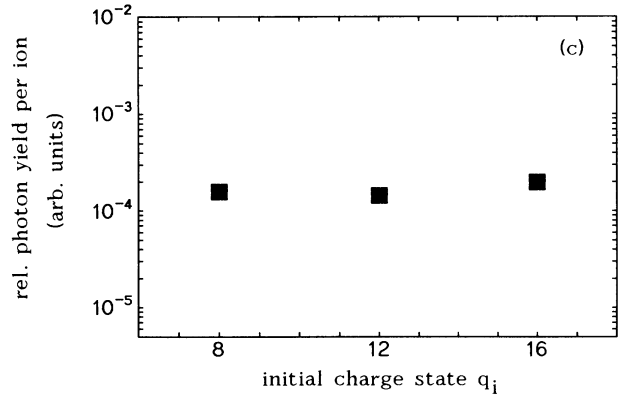

FIG. 8. (a) Relative fraction of the electron yield measured with the foil in position 1 (entrance yield) as a function of the projectile's initial charge state for the following repelling voltages V_R at the electron detector: $V_R = -100$ V (circles), $V_R = -150$ V (triangles), and $V_R = -200$ V (diamonds). The solid line represents the relative increase of the projectile's potential energy as function of its charge state q_i. (b) Relative fraction of the electron yield measured with the foil in position 2 (exit yield) as a function of q_i. The symbols represent the same repelling voltages V_R as in 8(a). (c) Relative fraction of the photon yield as a function of the initial projectile charge state measured with the foil in position 2.

excitation state independent of its incoming charge state. Furthermore, it was found that the relative electron exit yield is about equivalent to the entrance yield for incoming Ar^{8+}, which indicates that the ion's excitation state when leaving the foil is dominantly due to excitation processes in the foil rather than related to the excitation state of the incoming ion.

Figure 8(c) shows the yield of photons measured with foil in position 2 as a function of q_i. No q_i dependence can be observed. We assume those photons to be emitted in radiative deexcitation processes in the outgoing projectile. For the following reasons, we suspect that dominantly low-energy uv photons originating from transitions in outer shells are detected. First, radiative decay of inner-shell vacancies in Ar is very unlikely because of the small fluorescence yield [$\sim 5 \times 10^{-4}$ for neutral Ar (Ref. 34)] and second, the channel-plate detector has a relative high detection efficiency for uv photons. Since the lifetime of radiatively decaying excited outer-shell states is typically on the order of 10^{-9} sec,[34] one can conclude that the observed photon decay takes place behind the foil over a distance of several millimeters. The exit side electron yield has already shown that the ions have reached an equilibrium excitation state when leaving the foil. Therefore it is very reasonable to find no q_i dependence of the photon yield far behind the foil.

Figure 9 shows the distribution of final Ar charge states for those Ar ions that are detected coincidentally with an emitted photon from the exit surface. This distribution is clearly shifted to higher charge states relative to the total final charge-state distribution. We do not understand this finding. However, one could speculate that those Ar ions, which emit a photon behind the foil, undergo a close collision with a carbon atom shortly before they leave the foil, which leads to a higher degree of excitation and ionization relative to the total amount of outgoing Ar ions.

To summarize the main findings of the present experiment, one can say that a swift highly charged Ar ion

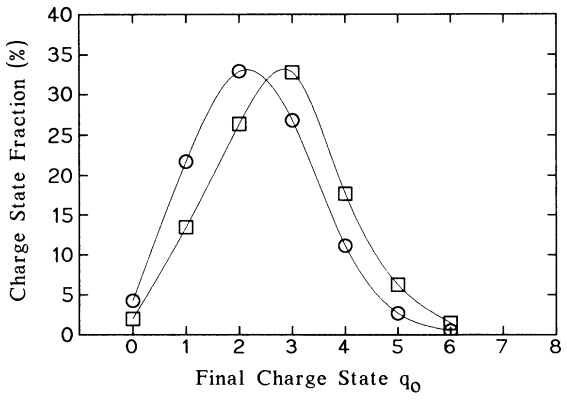

FIG. 9. Charge-state distribution of those outgoing projectiles that have emitted a photon after leaving the foil (squares). In comparison to that, the circles represent the total charge-state distribution of the outgoing projectiles. The initial charge state was $q_i = 16$.

($v_p = 0.76$ a.u.) that passes a carbon layer of 310 Å thickness leaves this foil in a charge and excitation state that does not "remember" at all its initial charge state. A model analysis of the energy-loss data leads to the conclusion that the ion reaches its equilibrium charge state immediately after penetrating into the carbon solid, after passing less than one atomic layer. In order to interpret those findings in terms of the populations of the ionic inner shells, electronic and nuclear energy loss may be treated separately. For electronic stopping, we would like to follow the description of Brandt.[35] The cloud of incident plus captured electrons that screens the projectile nucleus may extend to an average radius of $\Lambda(v_r)$, where v_r denotes the relative velocity between projectile and the conduction band electrons. Electrons in the medium with impact parameters $b_e > \Lambda(v_r)$ encounter the ion as point charge $Q(v_r) = q_i - N(v_r)$ in a distant collision, where q_i describes the projectiles incident charge state and $N(v_r)$ the number of captured electrons. Electrons at impact parameters $b_e < \Lambda(v_r)$ penetrate into the cloud of bound electrons and encounter in close collisions a partially screened potential corresponding to an ion charge that is larger than $Q(v_r)$. The projectile's effective ion charge Z^*, which arises from an average over all impact parameters and which determines the projectile's electronic energy loss, is therefore always larger than $Q(v_r)$, depending on the contributing fraction of collision processes with impact parameters $b_e < \Lambda(v_r)$. From a statistical treatment of steady-state electron capture and loss processes Brandt obtains $Q(v_r)$. Within the dielectric approximation for the stopping power, he evaluated the effective projectile charge state Z^* for nitrogen ions in several conducting solid targets. The effective charges extracted from measured stopping powers S by using the relation $S = S_p(Z^*)^2$, where S_p describes the corresponding proton stopping power, confirm his calculations in detail. Applying Brandt's formulas to our collision system leads to an average projectile screening radius of $\Lambda(v_r) = 0.2$ a.u. and to a ratio $Z^*/Q(v_r) = 1.33$. This shows that a considerable fraction of electronic stopping processes take place at impact parameters $b_e < 0.2$ a.u. The classical L-shell radius can roughly be estimated (in a.u.) as $r_L = n^2/(Z - m_k)$, where n is the main quantum number and m_k the number of screening electrons in the K shell. For Ar one obtains $r_L = 0.25$ a.u. According to those results one can conclude that the electronic stopping power in our collision system should depend on the average population in the projectile's L shell.

In order to obtain the impact parameter regime which contributes to nuclear stopping, classical Rutherford scattering between Ar and C is assumed. An average impact parameter $\langle b \rangle$, weight by its probability and the related energy loss $\Delta E(b)$ for nuclear collisions, is given by the following expressions:

$$\langle b \rangle = \frac{\int_o^{b_{\max}} b\,\Delta E(b)(dP/db)db}{\int_o^{b_{\max}} \Delta E(b)(dP/db)db} \quad \text{with } (dP/db) = 2\pi b \ . \tag{5}$$

$\Delta E(b)$ is, according to Rutherford's formula, given by

$$\Delta E(b) = \frac{2Q_1^2 Q_2^2}{M_2 v^2} \frac{1}{b^2 + (c/2)^2} \quad \text{with } c = \frac{Q_1 Q_2}{\frac{1}{2} M_o v^2} \ , \tag{6}$$

where Q_1 and Q_2 are the projectile and target charges, respectively. M_2 is the target mass and M_o is the reduced mass $M_o = (M_1 M_2)/(M_1 + M_2)$.

The evaluation of the above integrals leads to

$$\langle b \rangle = \frac{2\{b_{\max} - c/2[\arctan(2b_{\max}/c)]\}}{\ln[(b_{\max}^2 + c^2/4)/(c^2/4)]} \ . \tag{7}$$

The quantity c is called the collision diameter. For a repulsive interaction it describes the distance of the closest approach between the collision partners at zero impact parameter.

Since the projectile's energy loss $\Delta E(b)$ is maintained by assuming an unscreened Coulomb potential between the projectile and the target, a maximum impact parameter $b_{\max}$ as the upper integration limit in Eq. (5) has to be taken. Here we assumed $b_{\max} = 0.2$ a.u., according to the average projectiles screening radius $\Lambda(v_r)$ evaluated by Brandt.[35]

For the charge states of target and projectile, $Q_1 = 16$ and $Q_2 = 5$ were taken. These values consider some screening of the bare nuclear charges by the K-shell electrons and when inserted into the denominator of Eq. (5) lead to a total nuclear energy loss of the projectile in the 310-Å carbon foil of $\Delta E = 10.5$ keV, which is in good agreement with results of TRIM calculations.

According to Eq. (5), the average impact parameter $\langle b \rangle$ turns out to be $\langle b \rangle = 0.06$ a.u. The minimum internuclear distance $R_{\min}$, which is related with $\langle b \rangle$, is given by the relation

$$\langle R_{\min} \rangle = \frac{c}{2} + \sqrt{(c/2)^2 + \langle b \rangle^2} \ . \tag{8}$$

Inserting the values for c and b leads to $\langle R_{\min} \rangle = 0.069$ a.u. In the present case c is considerably smaller than $\langle b \rangle$ ($c = 0.016$). Therefore the values for $\langle R_{\min} \rangle$ and $\langle b \rangle$ are not very different.

$\langle R_{\min} \rangle$ is on the order of the Ar K-shell radius. The distance of closest approach, which is related to $b_{\max}$, is given by $R_{\min}(b_{\max}) = 0.208$ a.u. Since the Ar L-shell radius is roughly $r_L = 0.25$ a.u., we conclude that practically all energy transfer takes place in collisions closer than the Ar L-shell radius. Therefore, in the present collision system nuclear stopping should be very insensitive to the projectile and target electronic population outside the K shell.

On the other hand, the projectile's electronic energy loss should clearly depend on the electron population in the projectile's L shell. According to TRIM calculations, electronic stopping contributes by about 75% to the projectile's total energy loss. Therefore the Ar ion's total stopping power when passing the carbon foil should clearly vary with the number of electrons in the projectile's L shell. Since an incoming Ar^{8+} ion (filled L shell) and an Ar^{16+} ion (empty L shell) lead to the same total stopping power, one has to conclude that the

projectile's L shell is filled within the evaluated equilibration length.

In the following we discuss the possible mechanisms that might explain this finding. It was already described that, according to the currently established model, a highly charged ion starts to capture electrons from the conduction band of a surface into highly excited states in a surface distance of 10 Å. Only those electrons that have been transferred from these high n states into inner shells (typically $n \leq 3$) via Auger or radiative transitions in front of the surface remain captured in the ion when it penetrates into the solid. Electrons in higher-n states are "peeled off" upon penetration. The time of an Auger transition between two high-n states with $\Delta n = 1$ is typically $\Delta t = 6 \times 10^{-15}$ sec.[36] This time increases with increasing Δn. Typical radiative decay times are on the order of 10^{-9} sec for transitions between high-n states and 10^{-13} sec for inner-shell transitions. A transition cascade that can transfer an electron from a high-n state (typically $n \geq 7$) into an inner shell (L or K) of the ion can be estimated to take of the order of 10^{-14}–10^{-13} sec. During this time a 576-keV Ar ion has passed several hundreds of angstroms. Thus it can be concluded that capture into high-n states of the ion in front of the surface followed by Auger or radiative decay is a process that is too slow to populate efficiently inner shells of the ion. This conclusion is in full agreement with conclusions of various experiments that investigated electron and photon emission during interaction of highly charged ions with conducting surfaces.

Therefore one has to assume that the charge-exchange processes responsible for the very short projectile charge equilibration length observed in this experiment predominantly take place when the ion enters the solid. At this point, a very important filling process for the projectiles' inner-shell vacancies is the direct inner-shell electron transfer between the Ar and carbon core. At $v_p = 0.76$ a.u., inner-shell electron transfer between projectile and target can very well be described by using an adiabatic capture description such as the classical "over-barrier" or "molecular-orbital" model. Within these descriptions the electron transfer probability increases strongly with a decreasing energy separation between the involved electronic orbitals (energy matching condition). For neutral Ar, the Ar L and C K shell have very similar binding energies [for neutral atoms Ar (L_{I}) $E_b = 320$ eV, Ar (L_{II}) $E_b = 247$ eV, Ar (L_{III}) $E_b = 245$ eV, and C (K) $E_b = 284$ eV]. Therefore the electron transfer between these two orbits could be an important contribution to the total cross section for inner-shell electron transfer between Ar and C. In order to estimate the size of this contribution we refer to results of former experiments,[31] which have shown that for matching energies of the involved electronic orbitals and for adiabatic projectile velocities, electron transfer between the target and the projectile is very efficient within a range of internuclear distances in which the involved target and projectile electronic states have a spatial overlap. When applying those findings to the Ar-C system the maximum impact parameter at which an electron exchange between the C K shell and the Ar L shell occurs is obtained by adding the classical radii of both shells. This leads roughly to an impact parameter of $b \approx 0.2$ Å.

An estimation of the internuclear distance for capture out of the C K shell into Ar^{16+} by using the classical over-barrier model[37] leads to $b \approx 0.5$ Å. Within the accuracy that can be expected for the above-described geometric estimate, the agreement of both values seems reasonable. When assuming the probability for capture of one electron from the carbon K shell into the Ar projectile to be equal to one at internuclear distances smaller than $b = 0.5$ Å, one calculates a geometric cross section for the described capture of $\sigma \approx 0.8$ Å^2.

For a mean carbon density of 2.2 g/cm^3, the average distance between two carbon atoms in the foil is 2.1 Å, corresponding to one carbon atom in an area of 4.3 Å^2 in each layer. The probability P for a collision between an Ar ion and a C atom in one carbon layer in which the above-described electron transfer between the Ar L shell and the C K shell takes place is simply given by the ratio of both areas: $P = 0.8/4.3 = 0.19$. From this estimation one has to conclude that the Ar ion has to pass the order of five carbon layers for capturing one electron into the L shell. Therefore the described coupling between Ar L shell and the carbon K shell cannot be responsible for the very fast filling of Ar inner-shell vacancies.

Another possible relaxation process would be the Auger filling of the L shell after the ion enters the foil. The initial electrons could be transferred from the carbon K shell into the Ar M shell. We note that there is considerable momentum space overlap of the fast carbon K electrons not only with the Ar L shell, but also with the M shell. The corresponding Auger relaxation time is very difficult to model and we make no attempt to do so. We note that the width of a single L-hole vacancy in neutral Ar is of the order of 1 eV,[34] which would correspond to a lifetime of $T = 6 \times 10^{-16}$ sec or a flight path of about 10 Å. One would expect this lifetime to be shortened by the presence of more L vacancies, but lengthened by the absence of a full contingent of Ar M electrons on the moving ion. Whether T could be so short as to allow appreciable L filling in a single carbon layer is not evident to us.

We now summarize the results of our experiment. A highly charged Ar ion that passes a 310-Å carbon foil with an initial velocity of $v_p = 0.76$ a.u. leaves the foil in a charge and excitation state that does not depend on its initial charge state. The ion reaches its charge-state equilibrium after passing one layer of the solid. This very short equilibration length requires extremely fast charge-exchange processes between the ion and the solid. Inner-shell electron transfer between the carbon K shell and the Ar L shell does not seem to explain these findings.

ACKNOWLEDGMENTS

This work was supported by Volkswagenstiftung, Bundesministerium für Forschung und Technologie, Germany, and the Division of Chemical Sciences, Office of Basic Energy Sciences, Office of Basic Energy Research, U.S. Department of Energy.

[1] S. T. De Zwart, A. G. Drentje, A. L. Boers, and R. Morgenstern, Surf. Sci. **217**, 289 (1989).
[2] L. Folkerts and R. Morgenstern, Europhys. Lett. **13**, 377 (1990).
[3] F. W. Meyer, S. H. Overbury, C. C. Havener, P. A. Zeijlmans van Emmichhoven, and D. M. Zehener, Phys. Rev. Lett. **67**, 723 (1991).
[4] F. W. Meyer, S. H. Overbury, C. C. Havener, P. A. Zeijlmans van Emmichhoven, J. Burgdörfer, and D. M. Zeheener, Phys. Rev. A **44**, 7214 (1991).
[5] P. A. Zeijlmans van Emmichhoven, C. C. Havener, I. G. Hughes, D. M. Zehener, and F. W. Meyer, Phys. Rev. A **47**, 3998 (1993).
[6] K. Rohrbrück, K. Sommer, J. P. Biersack, J. Bleck-Neuhaus, S. Schippers, P. Roncin, D. Lecler, F. Fremont, and N. Stolterfoht, Phys. Rev. A **45**, 4653 (1992).
[7] F. W. Meyer, C. C. Havener, S. H. Overbury, K. J. Snowdown, D. M. Zehener, W. Heiland, and H. Hemme, Nucl. Instrum. Methods Phys. Res. B **23**, 234 (1987).
[8] K. J. Snowdon, C. C. Havener, F. W. Meyer, S. H. Overbury, D. M. Zehener, and W. Heiland, Phys. Rev. A **38**, 2294 (1988).
[9] S. Schippers, S. Hustedt, W. Heiland, R. Köhrbrück, J. Bleck-Neuhaus, J. Kemmler, D. Lecler, and N. Stolterfoht, Phys. Rev. A **46**, 4003 (1992).
[10] J. Das and R. Morgenstern, Phys. Rev. A **47**, R755 (1993).
[11] J. Das and R. Morgenstern, J. Phys. Condens. Matter **5**, A255 (1993).
[12] E. D. Donets, Phys. Scr. **T3**, 11 (1983).
[13] E. D. Donets, Nucl. Instrum. Methods Phys. Res. B **9**, 522 (1985).
[14] J. P. Briand, L. de Billy, P. Charles, S. Essabaa, P. Briand, R. Geller, J. P. Desclaux, S. Bliman, and C. Ristori, Phys. Rev. Lett. **65**, 159 (1990).
[15] J. P. Briand, L. de Billy, P. Charles, S. Essabaa, P. Briand, R. Geller, J. P. Desclaux, S. Bliman, and C. Ristori, Phys. Rev. A **43**, 565 (1991).
[16] M. W. Clarck, D. Schneider, D. Dewitt, J. W. Mc.Donald, R. Bruch, U. I. Safronova, I. Y. Tolstikhina, and R. Schuch, Phys. Rev. A **47**, 3983 (1993).
[17] M. Schulz, C. L. Cocke, S. Hagmann, M. Stöckli, and H. Schmidt-Böcking, Phys. Rev. A **44**, 1653 (1991).
[18] M. Delauny, S. Dousson, R. Geller, D. Hitz, P. Varga, and H. Winter, Phys. Rev. B **35**, 4232 (1987).
[19] M. Fehringer, M. Delauny, R. Geller, P. Varga, and H. Winter, Nucl. Instrum. Methods Phys. Res. B **23**, 245 (1987).
[20] M. Delauny, M. Fehringer, R. Geller, P. Varga, and H. Winter, Europhys. Lett. **4**, 377 (1987).
[21] G. Lakits, F. Aumayr, and H. Winter, Rev. Sci. Instrum. **60**, 3151 (1989).
[22] G. Lakits, F. Aumayr, and H. Winter, Phys. Rev. A **139**, 395 (1989).
[23] H. Kurz, K. Tögelhofer, H. Winter, F. Aumayr, and R. Mann, Phys. Rev. Lett. **69**, 1140 (1992).
[24] F. Aumayr, H. Kurz, K. Togelhöfer, and H. Winter, Nucl. Instrum. Methods, Phys. Rev. B **78**, 99 (1993).
[25] J. Burgdörfer, P. Lerner, and F. W. Meyer, Phys. Rev. A **44**, 5674 (1991).
[26] J. Burgdörfer and F. W. Meyer, Phys. Rev. A **47**, R20 (1993).
[27] H. Kurz, F. Aumayr, C. Lemell, K. Togelhöfer, and H. Winter, Phys. Rev. A **48**, 2182 (1993).
[28] J. D. Garcia, R. J. Fortner, and T. M. Kavanagh, Rev. Mod. Phys. **45**, 111 (1973).
[29] W. Brandt, Nucl. Instrum. Methods **191**, 453 (1981).
[30] J. F. Ziegler,J. P. Biersack, and U. Littmark, in *The Stopping and Range of Ions in Solids,* edited by J. F. Ziegler (Pergamon, New York, 1985).
[31] H. Schmidt-Böcking, M. H. Prior, R. Dörner, H. Berg, J. O. K. Pedersen, C. L. Cocke, M. Stöckli, and A. S. Schlachter, Phys. Rev. A **37**, 4640 (1989).
[32] P. Sigmund and K. B. Winterborn, Nucl. Instrum. Methods **119**, 541 (1974).
[33] S. Lencinas, J. Burgdörfer, J. Kemmler, O. Heil, K. Kroneberger, N. Keller, H. Rothard, and K. O. Groeneveld, Phys. Rev. A **41**, 1435 (1990).
[34] W. Bambynek, B. Craseman, R. W. Fink, H.-U. Freund, H. Mark, C. D. Swift, R. E. Price, and P. Venugopala Rao, Rev. Mod. Phys. **44**, 716 (1972).
[35] W. Brandt, Nucl. Instrum. Methods **194**, 13 (1982).
[36] R. D. Cowan, *The Theory of Atomic Structure and Spectra* (University of California Press, Berkeley, 1981).
[37] A. Niehaus, J. Phys. B **19**, 2925 (1986).